Available online at www.sciencedirect.com
ScienceDirect
Trans. Nonferrous Met. Soc. China 23(2013) 134−139
Transactions of Nonferrous Metals Society of China
www.tnmsc.cn

Nanostructured MnO_2 synthesized via methane gas reduction of manganese ore and hydrothermal precipitation methods

Davood MORADKHANI[1], Mahdieh MALEKZADEH[1, 2], Eltefat AHMADI[1, 2]

1. Faculty of Engineering, Islamic Azad University, Zanjan Branch, P.O. Box 45156-58145, Zanjan, Iran;
2. Research and Engineering Company for Non-ferrous Metals (RECo), P.O. Box 45195-1445, Zanjan, Iran

Received 2 February 2012; accepted 15 August 2012

Abstract: A three-stage methane gas (CH_4) reduction of manganese ore, dissolution, and precipitation from solution procedure was conducted to synthesize MnO_2 nanorods. Methane gas reduction was carried out at 850, 875, 900, 925, and 950 °C for 120 min. Precipitation of the α-MnO_2 nanorods was performed in the temperature range of 25−90 °C with a constant reaction time of 90 min. The morphology and particle size of the products were determined from scanning electron microscope (SEM) images and X-ray diffraction (XRD) patterns. The BET and BJH of the products were found out by the surface area analyzer. Reduction results indicated that MnO-rich phase is significantly formed at 950 °C as MnO_2 phase disappears. Precipitation results also showed an average diameter size of ~ 50 nm for the embedding α-MnO_2 nanorods with BET surface area of 174 m^2/g.
Key words: manganese dioxide; nanorods; methane gas reduction; precipitation

1 Introduction

One-dimensional (1D) nanostructures such as α-MnO_2 nanorods have attracted scientific interest due to their potential applications as conducting interconnectors, nanoscale electronic, optoelectronic, and sensing devices in various fields [1−5]. For instance, MnO_2 nanorods can be widely used as cathode materials both in aqueous and non-aqueous batteries like Li/MnO_2 batteries [6,7]. In addition, polymorphic forms of MnO_2, α-, β-, γ-, and δ-MnO_2, mainly different in the way of the basic unit [MnO_6] octahedral linked [8,9], have various electrochemical properties which depend on the crystalline structure and morphology of the oxide. Results disclose that nanostructured α-MnO_2 and δ-MnO_2 can admit a considerable amount of lithium ions in their structures [2−5, 8−10]. Thus, a large capacity of rechargeable lithium batteries can be prepared by using cathode materials made of nanostructured α-MnO_2 and δ-MnO_2 [6−11].

Although δ-MnO_2 can be used as a cathode material, it is a two-dimensional type of manganese dioxide which shows lower surface area in comparison with α-MnO_2 [2,5,8,9,12−14]. One-dimensional (1D) α-MnO_2 nanorods can be synthesized either by electrochemical or by hydrothermal/solvothermal methods [5,4−13]. The majority of these procedures are based on the hydrothermal methods such as chemical reduction, sonochemical procedures, and sol-gel synthetic route [7,11−13]. Previous studies have been confined to the preparation of the nanostructured MnO_2 by using analytical grade materials as raw materials [5−8, 10−23].

The authors are not aware of any literature data on the direct synthesis of nanostructured MnO_2 from pyrolusite type of the manganese ore. In the present work, manganese dioxide nanorods were synthesized by taking the advantages of methane gas reduction of pyrolusite ore and precipitating of the α-MnO_2 nanorods from the aqueous solution obtained from leaching step of MnO in sulfuric acid under optimum conditions.

The purpose of this investigation is to elucidate the results of synthesizing the single phase α-MnO_2 nanorods by means of hydrothermal route using pyrolusite type ore as a raw material due to the affluence of the natural manganese resources. The important preparation parameters such as methane gas reduction temperature of pyrolusite ore and precipitation temperature of nanostructured MnO_2 from manganese sulfate solutions are also clarified in this work. Phase

Corresponding author: Eltefat AHMADI; E-mail: elt_ahmadi@alum.sharif. edu; elt_ahmadi@yahoo.com
DOI: 10.1016/S1003-6326(13)62439-5

transformation, morphological and structural evolution of the samples are precisely considered by XRD, SEM, and BET analysis.

2 Experimental

A three-stage methane gas reduction of the manganese ore, dissolution, and precipitation from solution procedure were carried out to synthesize nanostructured MnO_2 rods. Typical analysis of the manganese ore which was determined by XRD and XRF methods was as follows (mass fraction): Mn <40%; TiO_2 <0.2%; Al_2O_3 <15%; Fe_2O_3 <4%; CaO <3%; SiO_2 <10%. Initially, manganese ore was crushed to the size fraction of 3−5 μm and reduced isothermally by a flow of about 0.5 L/min gaseous methane in a fixed bed reactor utilizing recrystallized alumina boats. The boat load weighed 10 g with a height of 5 mm. Methane gas reduction tests were performed at different temperatures: 850, 875, 900, 925, and 950 °C for 120 min with purified methane gas. Next, dissolution step was carried out for 90 min in 250 mL of 1 mol/L H_2SO_4 solution at temperature of about 80 °C to prepare manganese sulfate solution with the Mn concentration of 43.94 g/L. Subsequently, the synthesized solution was heated up to the required temperatures under continuous electromagnetic stirring. The stirring rate remained constant during each test and was about 250 r/min. Finally, in the precipitation stage, the solution was fed with 250 mL of aqueous ammonium persulfate solution (0.7 mol/L) at different temperatures in the range of 25 to 90 °C for 90 min to precipitate α-MnO_2 nanorods. After reaction for 90 min, the precipitates were filtered and rinsed with distilled water and ethanol to remove any chemical species possibly remaining in the final products and kept in ethanol. Phase transformation, morphological, and structure evolution of the samples and particle size of the products were also rigorously considered by X-ray diffraction (XRD, Powder Metallurgy 9920/50, Philips, Holland), scanning electron microscope (SEM, VEGA, TESCAN Czech Republic). The BET specific surface area was determined by nitrogen adsorption at 77 K using a surface area analyzer (Micromeritics ASAP 2000 system).

3 Results and discussion

Among manganese oxides (MnO, Mn_3O_4, Mn_2O_3, and MnO_2), MnO has a strong capability of dissolution in sulfuric acid media [24,25]. Thus, the reduction processes of the manganese ore containing MnO_2 phase and small amount of other oxides were conducted in methane gas (CH_4) to obtain MnO phase. Manganese sulfate solution, being utilized in precipitation stage, was produced by the dissolution of MnO in sulfuric acid media. The reduced ores were dissolved under an optimum condition to obtain desirable $MnSO_4$ solution with the concentration of about 43.94 g/L Mn. Subsequently, precipitation step of MnO_2 nanorods was carried out using aqueous ammonium persulfate ($(NH_4)_2S_2O_8$). Figure 1 exhibits the XRD patterns of the manganese ore after the methane gas reduction process at five different temperatures of 850, 875, 900, 925, and 950 °C for 120 min. The formation of MnO phase as well as intermediate phases was investigated rigorously. The XRD pattern of the raw manganese ore is presented in Fig. 1 also. It is clear that the peaks of raw manganese observed in Fig. 1 belong to MnO_2, Mn_2O_3, Mn_2SiO_4, SiO_2, $CaCO_3$ and small amount of iron oxides. Considering the fact that MnO phase has strong capability of dissolution in sulfuric acid, the reduction process of the manganese ore was carried out to yield the MnO-rich phase.

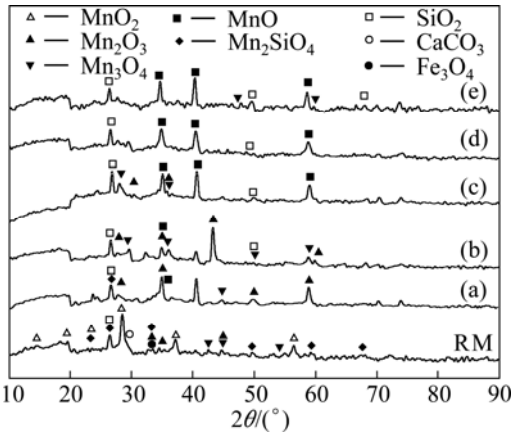

Fig. 1 XRD patterns of methane gas reduced ores at different temperatures for 120 min: (RM) raw manganese ore; (a) 850 °C; (b) 875 °C; (c) 900 °C; (d) 925 °C; (e) 950 °C

As can be seen from Fig. 1, increasing the reduction temperature resulted in decreasing the ratio of oxygen to manganese in the samples. The XRD patterns of the manganese ores partially reduced at temperatures of 850 and 875 °C are represented in Figs. 1(a) and (b). Clearly, it can be seen that the formation of MnO phase started slightly at the reduction temperature about 875 °C. Figs. 1(c)−(e) demonstrate that by increasing the reduction temperature from 900 to 950 °C, the amount of intermediate phases decreased and the amount of MnO phase increased. Eventually, MnO-rich phase was completely formed at the temperature of 950 °C as MnO_2 phase disappeared.

From the XRD results presented in Fig. 1, the reduction of MnO_2 to MnO follows the sequence:

$$MnO_2 \rightarrow Mn_2O_3 \rightarrow Mn_3O_4 \rightarrow MnO \quad (1)$$

Not only does heating the manganese ore under methane gas result in decomposing of MnO_2 phase and forming of Mn_2O_3 (bixbyte) phase, but also Mn_2O_3 transfers to Mn_3O_4 (hausmannite) at temperature above 850 °C as well. The corresponding reactions for the reduction of MnO_2 and formation of MnO from MnO_2 phase in methane gas (CH_4) can be summarized by the following reactions [26−29]:

$$8MnO_2(s)+CH_4(g) \rightarrow 4Mn_2O_3(s)+2H_2O(g)+CO_2(g) \quad (2)$$

$$12Mn_2O_3(s)+CH_4(g) \rightarrow 8Mn_3O_4(s)+CO_2(g)+2H_2O(g) \quad (3)$$

$$4Mn_3O_4(s)+CH_4(g) \rightarrow 12MnO(s)+CO_2(g)+2H_2O(g) \quad (4)$$

The sum of the three reactions is as follows:

$$4MnO_2(s)+CH_4(g) \rightarrow 4MnO(s)+2H_2O(g)+CO_2(g) \quad (5)$$

The standard Gibbs free energy change (ΔG^{Θ}_{298}) of reactions (2)−(5) can be determined from ΔH^{Θ}_{298} and ΔS^{Θ}_{298} data of compounds and elements (Table 1). The thermodynamic data show that the relevant ΔG^{Θ} values for the reduction of Mn_2O_3 are more negative than those calculated for the reduction of Mn_3O_4; on the other hand, Mn_2O_3 could be very easily reduced to MnO phase [26−29].

Table 1 Thermodynamic properties of manganese and manganese oxides at 298 K and 1.01×10^5 Pa [26−29]

Metal/oxide	ΔH^{Θ}_{298} /(kJ·mol^{-1})	ΔS^{Θ}_{298} /(kJ·mol^{-1}K^{-1})
Mn	0	31.98±0.084
MnO	−384.56±2.09	59.77±0.084
Mn_3O_4	−1385.25±4.18	153.82±3.34
Mn_2O_3	−955.97±5.02	110.35±0.21
MnO_2	519.57±2.09	53.09±0.42

The conversion of methane gas (CH_4) to CO_2 as a function of temperature for different oxygen carrier materials was considered by HOSSAIN and LASA [30]. These authors reported a possible choice of oxygen carrier materials based on thermodynamics data for the reduction of some common materials using methane gas as the reducing agent in the temperature range of 600−1200 °C. It has been shown that MnO_2/Mn_2O_3, Mn_2O_3/Mn_3O_4, Co_3O_4/CoO and CuO/Cu_2O have greater tendency to react with methane as compared to Fe_2O_3/Fe_3O_4 and NiO/Ni; and MnO_2, Mn_2O_3, Co_3O_4 and CuO decompose into Mn_2O_3, Mn_3O_4, CoO and Cu_2O, respectively, at low temperatures. MATTISSON and LYNGFELT [31] analyzed the kinetics data and found that Mn_2O_3/Mn_3O_4, CuO/Cu_2O, Fe_2O_3/Fe_3O_4 and NiO/Ni carrier materials are able to convert CH_4 to CO_2 almost completely. Not only are these oxygen carrier materials able to convert CH_4 to CO_2 entirely, but also carbon formation is a possible side reaction in chemical reduction processes under gaseous atmospheres accomplished by Boudouard reaction [29,30]. The conversion of CH_4 has also been studied by other researchers, and their results have verified the decomposition of CH_4 into the carbon and hydrogen as the following reaction [32]:

$$CH_4 \rightarrow 2H_2+C(s),\ \Delta G^{\Theta}_{298}=-38\ \text{kJ/mol},\ \Delta H^{\Theta}_{298}=88\ \text{kJ/mol} \quad (6)$$

Therefore, the reduction process of manganese dioxide starts with the adsorption of methane gas on the active sites of the oxide surface and its decomposition to reducing agents. The methane gas-reduced ore at above 950 °C consists merely of MnO phase without considerable amount of the intermediate phases (Fig. 1). To acquire manganese sulfate solution ($MnSO_4$), dissolving experiments were carried out in a 1 L cylindrical container immersed into a thermostatically controlled water bath. Practically, leaching step timed 90 min in 250 mL of 1 mol/L H_2SO_4 solution at temperature of about 80 °C to prepare manganese sulfate solution with the Mn concentration of 43.94 g/L. Then, manganese sulfate solutions were oxidized to form manganese dioxide (MnO_2) using ammonium persulfate ($(NH_4)_2S_2O_8$) solution as [2,9−13]

$$MnSO_4+(NH_4)_2S_2O_8+H_2O \rightarrow MnO_2+(NH_4)_2SO_4+2H_2SO_4 \quad (7)$$

Figure 2 indicates the representative SEM images of MnO_2 powders synthesized by an aqueous reaction between manganese sulfate ($MnSO_4$) and ammonium persulfate ($(NH_4)_2S_2O_8$) at different temperatures with a constant reaction time of 90 min. It can be seen from Fig. 2(a) that the MnO_2 powders synthesized at room temperature show aggregated cactus-shaped nano-spheres/clusters consisting of nanorods intertwined with diameter of 400−600 nm.

As presented in Figs. 2(a)−(d), morphological changes accompanied with cluster/particle size shrinking occurred with increasing the reaction temperature. When the reaction temperature (RT) increased to 50, 70, and 90 °C, the cactus-shaped nano-spheres/clusters inclined to smash up and nanorodes can be formed. Hence, at 90 °C, nano-spheres/clusters (γ-MnO_2) can be hardly seen. By means of SEM wall to wall tool, the mean size of the nano-clusters was determined to be ~300 nm; the mean diameter and length of the embedding nanorods were also estimated to be about 50 and 100 nm, respectively.

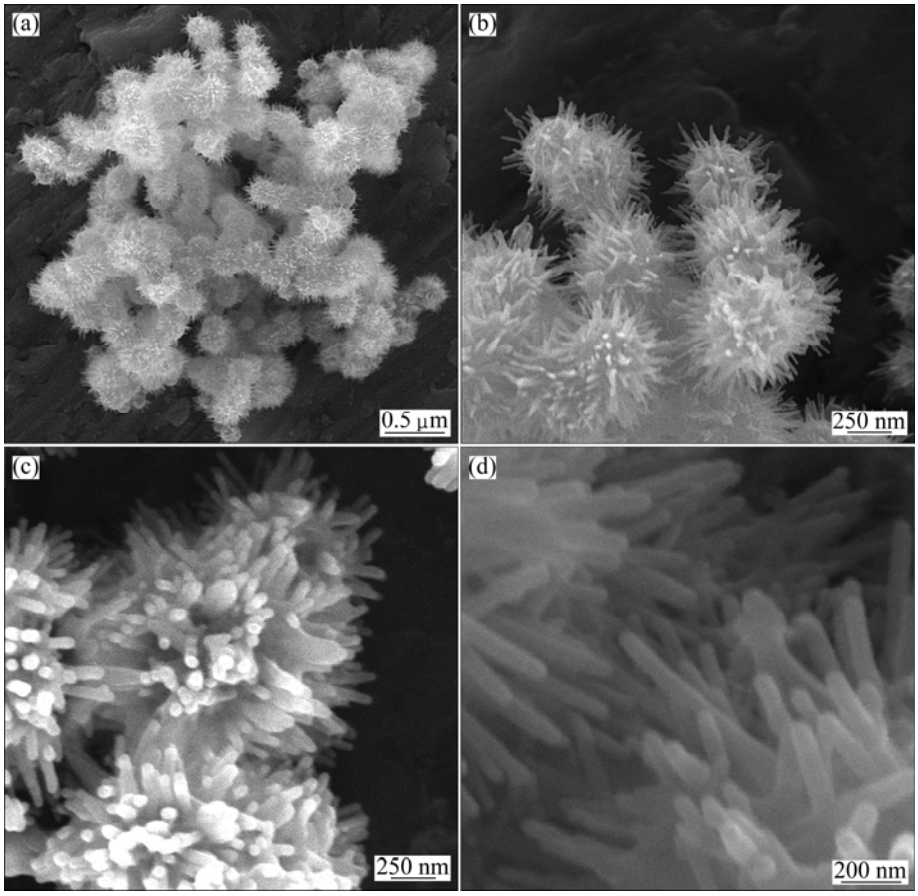

Fig. 2 SEM images of MnO_2 powders prepared at different temperatures with reaction time of 90 min: (a) Room temperature; (b) 50 °C; (c) 70 °C; (d) 90 °C

The XRD patterns of MnO_2 powders synthesized at 25 and 90 °C for 90 min are given in Fig. 3. The XRD graphs exhibit γ-MnO_2 and α-MnO_2 phases at 25 and 90 °C, respectively. Furthermore, the XRD results (Fig. 3) substantiate the transformation of the γ-MnO_2 phase to α-MnO_2 nanorods by increasing reaction temperature from room temperature to 90 °C. The morphological and structural evolution of the α-MnO_2 nanorods synthesized via an aqueous route through MnO_4^-/Mn_2^+ reaction was studied by FU et al [2]. They deduced that increasing the reaction temperature from room to higher temperatures results in progressive transformation of γ-MnO_2 to α-MnO_2 crystallites. Williamson-Hall correlation was used to determine the average crystallite size of the α-MnO_2 nanorods.

$$b\cos\theta = \frac{0.9\lambda}{d} + 2\varepsilon\sin\theta \quad (8)$$

where b is the width of the full peak at half intensity (rad), θ shows the position of the peak in the pattern (rad), λ is the wavelength of the X-ray (nm), d is the average size of the crystallites and ε is the micro-strain in the powder. The average crystallite size obtained from XRD results was well consistent with the average

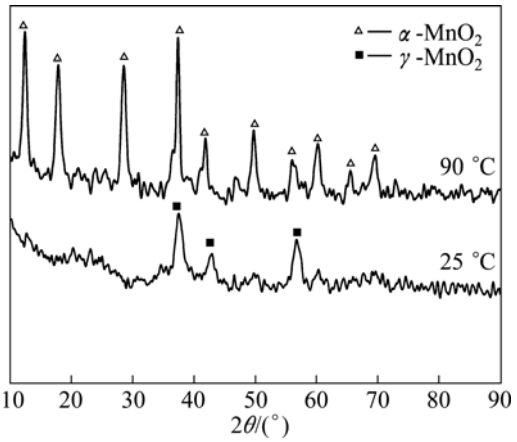

Fig. 3 XRD patterns of MnO_2 powders synthesized at 25 and 90 °C for 90 min

crystallite size found from SEM images, specifically α-MnO_2 nanorods. It is estimated to be about (53±5.0) nm for α-MnO_2 nanorods prepared at 90 °C.

The N_2 absorption-desorption isotherms of the samples were also measured by using the static volumetric absorption analyzer. The specific surface area of MnO_2 nanopowders was calculated using multipoint BET-equation. The S_{BET} (BET surface area) of

nanostructured MnO_2 was plotted with respect to the reaction temperatures (Fig. 4). It is evident from Fig. 4 that with increasing the reaction temperature, the S_{BET} of the synthesized powders increases remarkably. This is due to the phase transformation of γ-MnO_2 phase to α-MnO_2 nanorods that entirely occurs at higher temperatures.

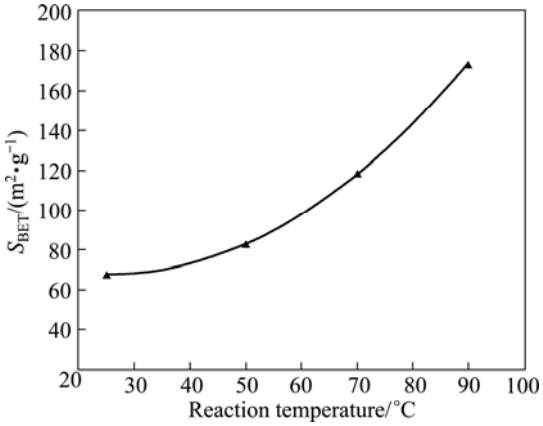

Fig. 4 BET surface area of MnO_2 nanopowders synthesized at different temperatures

Figure 5 indicates the comparison of the typical BJH pore size distribution curves of MnO_2 nanopowders synthesized at 25 and 90 °C. The results of BJH analysis exhibit that the pore size distribution of γ-MnO_2 and α-MnO_2 produced at 25 and 90 °C was very narrow and centered at 135 and 52 nm, respectively. The curves confirm a homogeneous distribution of uniform nanopores. It also demonstrates that most of the nanopores interposed in α-MnO_2 nanorods are smaller than 100 nm which affect the catalytic activities of MnO_2 nanorods, significantly.

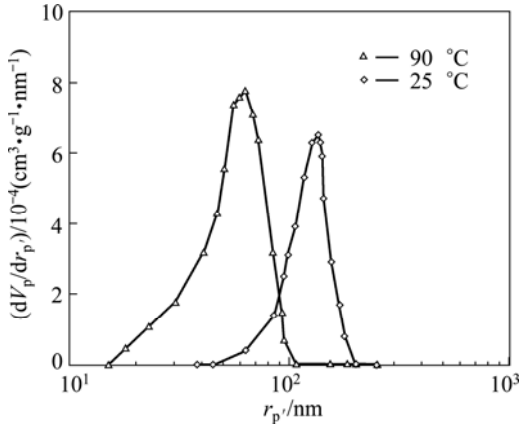

Fig. 5 BJH pore size distribution curves of MnO_2 nanopowders synthesized at different temperatures

4 Conclusions

Methane gas (CH_4) reduction, dissolution, and precipitation processes were employed to synthesize nanostructured α-MnO_2 rods. The reduction results demonstrated that MnO phase, the proper phase to acquire manganese sulfate solution ($MnSO_4$), is a dominant phase emerged from the reduction process above 950 °C. The α-MnO_2 nanorods with a mean diameter of about 50 nm were synthesized via an aqueous reaction between manganese sulfate, obtained from dissolution process, and ammonium persulfate ($(NH_4)_2S_2O_8$) at 90 °C within reaction time of 90 min. BET results showed that the specimens precipitated at 90 °C for 90 min had the highest surface area (S_{BET}~174 m^2/g). Furthermore, the pore size distribution of the α-MnO_2 nanorods was narrow and centered at 52 nm that significantly impacts catalytic behavior of MnO_2 nanostructures utilized as cathode materials.

Acknowledgements

The authors would like to thank the financial supports of the Islamic Azad University of Zanjan.

References

[1] CAO Y L, YANG H X, AI X P, XIAO L F. The mechanism of oxygen reduction on MnO_2-catalyzed air cathode in alkaline solution [J]. Journal of Electroanalytical Chemistry, 2003, 557: 127−134.

[2] FU X, FENG J, WANG H, NG K M. Morphological and structural evolution of α-MnO_2 nanorods synthesized via an aqueous route through MnO_4^-/Mn^{2+} reaction [J]. Journal of Solid State Chemistry, 2010, 183: 883−889.

[3] XU N, LIU Z H, MA X, QIAO S, YUAN J. Controlled synthesis and characterization of layered manganese oxide nanostructures with different morphologies [J]. Journal of Nanoparticle Research, 2009, 11: 1107−115.

[4] HE X, YANG M, NI P, LI Y, LIU ZH. Rapid synthesis of hollow structured MnO_2 microspheres and their capacitance [J]. Colloids and Surfaces A: Physicochemical and Engineering Aspects, 2010, 363: 64−70.

[5] YANG Z, ZHOU C, ZHANG W, LI H, CHEN M. β-MnO_2 nanorods: A new and efficient catalyst for isoamyl acetate synthesis [J]. Colloids and Surfaces A: Physicochemical and Engineering Aspects, 2010, 356: 134−139.

[6] SUGANTHA M, RAMAKRISHNAN P A, HERMANN A M, WARMSINGH C P, GINLEY D S. Nanostructured MnO_2 for Li batteries [J]. International Journal of Hydrogen Energy, 2003, 28: 597−600.

[7] ORLOV A, GRABIS J, KRUMINA A, RASMANE D, JANKOVICA D, HEIDEMANE G. Li-containing oxide nanopowders prepared by the plasma chemical synthesis [J]. Materials Science, 2005, 11: 38−44.

[8] LI Q W, LUO G, LI J, XIA X. Preparation of ultrafine MnO_2 powders by the solid state method reaction of $KMnO_4$ with Mn (II) salts at room temperature [J]. Journal of Materials Processing Technology, 2003, 173: 25−29.

[9] LIN H Y, SUN Y P, WENG B J, YANG C T, SUEN N T, LIAO K H, HUANG Y C, HO J Y, CHONG N S, TANG H Y. Factors influencing the structure of electrochemically prepared α-MnO_2 and γ-MnO_2 phases [J]. Electrochimica Acta, 2007, 52: 6548−6553.

[10] LI Y, ZHOU X, ZHOU H, SHEN Z, CHEN T. Hydrothermal preparation of nanostructured MnO_2 and morphological and

crystalline evolution [J]. Frontiers of Chemistry in China, 2008, 3(2): 128−132.
[11] YU P, ZHANG X, CHEN Y, MA Y. Solution-combustion synthesis of ε-MnO_2 for supercapacitors [J]. Materials Letters, 2010, 64: 61−64.
[12] WANG N, PANG H, PENG H, LI G, CHEN X. Hydrothermal synthesis and electrochemical properties of MnO_2 nanostructures [J]. Crystal Research and Technology, 2009, 44: 1230−1234.
[13] YUE G H, YAN P X, YAN D, QU D M, FAN X Y, WANG M X, SHANG H T. Solvothermal route synthesis of single-crystalline α-MnO_2 nanowires [J]. Journal of Crystal Growth, 2006, 294: 385−388.
[14] ZHAO L, WANG R. γ-MnO_2 nano-sieve membrane: Preparation, characterization and reaction studies [J]. Applied Surface Science, 2004, 236: 217−222.
[15] XU F, WANG T, LI W, JIANG Z. Preparing ultra-thin nano-MnO_2 electrodes using computer jet-printing method [J]. Chemical Physics Letters, 2003, 375: 247−51.
[16] HE W L, ZHANG Y C, ZHANG X X, WANG H, YAN H. Low temperature preparation of nanocrystalline Mn_2O_3 via ethanol-thermal reduction of MnO_2 [J]. Journal of Crystal Growth, 2003, 252: 285−288.
[17] KUMAR V G, KIM K B. Organized and highly dispersed growth of MnO_2 nano-rods by sonochemical hydrolysis of Mn (3) acetate [J]. Ultrasonics Sonochemistry, 2006, 13: 549−556.
[18] MAZUR M, GONTARZ Z. Reactions of manganese oxides with $K_2S_2O_7$ [J]. Journal of Thermal Analysis and Calorimetry, 2009, 10: 993−998.
[19] SHARMA R K, OH H S, SHUL Y G, KIM H. Growth and characterization of carbon-supported MnO_2 nanorods for super capacitor electrode [J]. Physica B, 2008, 403: 1763−1769.
[20] KIM H, POPOV B N. Synthesis and characterization of MnO_2-based mixed oxides as super capacitors [J]. Journal of the Electrochemical Society, 2003, 150(3): 56−62.
[21] LI J, WANG X, HUANG Q, GAMBOA S, SEBASTIAN PJ. A new type of $MnO_2{\cdot}xH_2O$/CRF composite electrode for super capacitors [J]. Journal of Power Sources, 2006, 160: 1501−1505.
[22] TENG F, SANTHANAGOPALAN S, MENG D D. Microstructure control of MnO_2/CNT hybrids under in-situ hydrothermal conditions [J]. Solid State Sciences, 2010, 12: 1677−1682.
[23] LIU M, ZHAN G J, SHEN Z R, SUN P C, DING D T, CHEN T H. Synthesis and characterization of hierarchically structured mesoporous MnO_2 and Mn_2O_3 [J]. Solid State Sciences, 2009, 11: 118−128.
[24] WELHAM N J. Activation of the carbothermic reduction of manganese ore [J]. International Journal of Mineral Processing, 2002, 67: 187−198.
[25] NAYAK B B, MISHRA K G, PARAMGURU R K. Kinetics and mechanism of MnO_2 dissolution in H_2SO_4 in the presence of pyrite [J]. Journal of Applied Electrochemistry, 2009, 29: 191−200.
[26] KONONOV R, OSTROVSKI O, GANGULY S. Carbothermal reduction of manganese oxide in different gas atmospheres [J]. Metallurgical and Materials Transaction B, 2008, 39: 662−668.
[27] OSTROVSKI O, ANACLETO N, GANGULY S. Reduction of manganese ores by methane- containing gas [C]//Proceedings of the Tenth International Ferroalloys Congress. Cape Town, South Africa: Document Transformation Technologies, 2004: 173−183.
[28] ANACLETO N, OSTROVSKI O, GANGULY S. Reduction of manganese ores by methane containing gas [J]. ISIJ International, 2004, 44: 1480−1487.
[29] LIDE D R. CRC Handbook of Chemistry and Physics [M]. 89th Edition. CRC Press, 2008.
[30] HOSSAIN M M, de LASA H I. Chemical-looping combustion (CLC) for inherent CO_2 separations—A review [J]. Chemical Engineering Science, 2008, 63: 4433−4451.
[31] MATTISSON T, LYNGFELT A. Capture of CO_2 using chemical-looping combustion [C]//Proceedings of First Biennial Meeting of the Scandinavian-Nordic Section of the Combustion Institute. Goteborg, Sweden, 2001.
[32] BAUTISTA O, MENDEZ F, TREVINO C. Theoretical analysis of the direct decomposition of methane gas in a laminar stagnation-point flow: CO_2-free production of hydrogen [J]. International Journal of Hydrogen Energy, 2008, 33: 7419−7426.

甲烷气体还原锰矿和水热沉淀法制备纳米 MnO_2

Davood MORADKHANI[1], Mahdieh MALEKZADEH[1, 2], Eltefat AHMADI[1, 2]

1. Faculty of Engineering, Islamic Azad University, Zanjan Branch, P.O. Box 45156-58145, Zanjan, Iran;
2. Research and Engineering Company for Non-ferrous Metals (RECo), P.O. Box 45195-1445, Zanjan, Iran

摘　要：采用甲烷气体还原锰矿、溶解和水热沉淀方法制备 MnO_2 纳米棒。甲烷气体还原反应在 850、875、900、925 和 950 ℃ 下进行 120 min，生成 α-MnO_2 纳米棒的沉淀反应在 25~90 ℃ 下进行 90 min。采用 SEM 和 X 射线衍射对制备的产物形貌和颗粒尺寸进行表征。采用比表面分析仪测定产物的 BET 和 BJH 值。结果表明，在反应温度 950 ℃ 下，MnO 相大量生成，而 MnO_2 相消失。所制备的 α-MnO_2 纳米棒的平均直径约为 50 mm，其 BET 比表面积为 174 m^2/g。

关键词：二氧化锰；纳米棒；甲烷气体还原；沉淀反应

(Edited by Sai-qian YUAN)